

1 **Synergies, radiation and kinetics in photo-Fenton process with UVA-LEDs**

2 N. López-Vinent, A. Cruz-Alcalde, L.E. Romero, M.E. Chávez, P. Marco, J. Giménez\*,  
3 S. Esplugas

4

5 *Department of Chemical Engineering and Analytical Chemistry, Faculty of Chemistry,*  
6 *Universitat de Barcelona, C/Martí i Franqués 1, 08028 - Barcelona, Spain. Tel:*  
7 *+34934021293. Fax: +34934021291*

8 \*Corresponding Author: *j.gimenez.fa@ub.edu*

9 **ABSTRACT**

10 The photo-Fenton process, with UV-A LED ( $\lambda=380-390$ ,  $390-400$  and  $380-400$  nm) has  
11 demonstrated to be effective in the abatement of a target micropollutant, such as  
12 diphenhydramine hydrochloride (DPH). Different concentrations of iron ( $\text{Fe}^{2+}$ ) and  $\text{H}_2\text{O}_2$   
13 were tested and monitored, and the best results in DPH removal were obtained for the  
14 highest concentrations of both iron (II) and  $\text{H}_2\text{O}_2$  (10 mg  $\text{Fe}^{2+}/\text{L}$  - 150 mg  $\text{H}_2\text{O}_2/\text{L}$ ). The  
15 evolution of iron and peroxide concentration was also monitored. Kinetic studies showed  
16 that dark Fenton process prevails at the beginning of the experiment, when  $\text{Fe}^{2+}$   
17 concentration is higher. However, after these initial moments, the prevailing process is  
18 photo-Fenton and, in addition, wavelength radiation plays an important role. Concerning  
19 the effect of radiation, four LEDs (4.2 W total power) were used, emitting radiation in the  
20 wavelength range between 380-390 or 390-400 nm. Similar results were obtained in both  
21 cases in DPH removal by photo-Fenton (30 min for total elimination). However, a  
22 synergistic effect was observed when two LEDs of 380-390 nm and two LEDs of 390-  
23 400 nm were used. Total power was the same (4.2 W) in each experimental condition,  
24 but the increase in the wavelength range to 20 nm (380-400 nm) produces an increase in

25 the rate of DPH removal, achieving its total elimination at 15 min. This fact, with the use  
26 of a simple radiation model, reveals the important role that radiation plays in the photo-  
27 Fenton process. Finally, the formed intermediates were determined and some reaction  
28 pathways were proposed.

## 29 **KEYWORDS**

30 Synergy wavelength, UV-A LED, photo-Fenton, Intermediates, Kinetics

## 31 **1. INTRODUCTION**

32 Micropollutants (MPs), especially pharmaceuticals, have been an increasing concern due  
33 to their biorecalcitrant character. Because of that property, MPs are not completely  
34 eliminated during conventional wastewater treatments [1]. Moreover, they potentially  
35 affect human health as a consequence of long-term exposure [2]. Important amounts of  
36 pharmaceuticals are used, but there is little concern about the final disposal of these drugs.  
37 In Deo's study [3], a risk index (RQ) was calculated for numerous micropollutants, related  
38 to the impact on the aquatic ecosystem. According to RQ, pharmaceuticals are classified  
39 in three categories: high risk ( $RQ \geq 1.0$ ), medium risk ( $1.0 > RQ \geq 0.1$ ) or low risk ( $RQ < 0.1$ ).  
40 In this work, the pharmaceutical diphenhydramine hydrochloride (DPH), with RQ 0.39,  
41 has been chosen as a model compound. DPH is an antihistaminic drug that has been  
42 detected in surface waters in concentrations around 1.40  $\mu\text{g/L}$ .

43 Advanced Oxidation Processes (AOPs) are effective options for the removal of emerging  
44 and recalcitrant contaminants from wastewaters [4-9]. Among AOPs, the photo-Fenton  
45 process has demonstrated to be effective in the abatement of MPs. In this process, a  
46 catalytic cycle with iron (II and III), hydrogen peroxide ( $\text{H}_2\text{O}_2$ ) and ultraviolet (UV) light  
47 are combined to generate hydroxyl radicals ( $\text{HO}\cdot$ ) [10].

48 Photochemical processes present several disadvantages due to the cost and electrical  
49 consumption of the UV lamps [11]. Numerous studies based on AOPs use mercury lamps  
50 as a source of UV light, presenting diverse drawbacks, like high power consumption [12]  
51 and a low lifetime and overheating problems [13, 14]. In addition, they present problems  
52 associated with its disposal [15, 16] due to the mercury content. In this sense, the  
53 Minamata Convention on Mercury has been approved by 128 countries in an attempt to  
54 remove mercury from several products and methods by 2020 [17].

55 Due to all these disadvantages, UV light-emitting diodes (UV-LEDs), as potential  
56 substitutes, have been tested in numerous studies with AOPs [18, 19]. Contrary to  
57 traditional mercury lamps, UV-LEDs offer low energy consumption, long lifetime, small  
58 size, no mercury content, no problems associated with overheating and the possibility of  
59 selecting specific wavelengths and reaction configurations according to particular needs  
60 [20, 21]. In spite of the numerous advantages that LEDs may provide, the use of mercury  
61 lamps is still a cheaper option nowadays as conventional lamps are really efficient in the  
62 conversion of electricity to light. Thus, improvements in the efficiency and power are  
63 required to apply LED radiation sources in AOPs. Hölz and coworkers [22] studied the  
64 replacement of mercury lamps by LEDs in photochemistry applications. A comparison in  
65 terms of consumption and costs was conducted between both radiation sources. The  
66 investigation revealed that electricity (kWh/year) (value of 30 instead of 2600 kWh/year  
67 in LEDs and mercury lamps, respectively), initial cost (€) (12,000 € for LEDs and 1,500  
68 € for mercury lamps) and consumables (€/year) (50 €/year for LEDs instead 2,400 €/year  
69 for mercury lamps) could be potentially lower in LEDs than in mercury lamps, provided  
70 that the type of LED technology required in the photochemistry area is upgraded in terms  
71 of energy conversion efficiency.

72

73 The aim of this study was to test the efficiency of UV-A LED photo-Fenton process in  
74 DPH degradation. The effect of hydrogen peroxide ( $\text{H}_2\text{O}_2$ ) and initial iron ( $\text{Fe}^{2+}$ )  
75 concentrations on DPH removal was studied. LEDs with different wavelength ranges  
76 (380-390 nm and 390-400 nm) were used and the synergistic effect was also studied and  
77 explained by using a simple radiation model. Additionally, reaction pathways were  
78 proposed according to detected reaction intermediates. Although the application of photo-  
79 Fenton for MPs abatement is currently a hot research topic, further research including the  
80 use of LEDs is still needed for process intensification. In this work, the use of two  
81 wavelengths has been evaluated, and potential synergistic effects explored. The study of  
82 synergistic effect is a novel part of this paper because this is not a common topic when  
83 LEDs are used. In addition, the novelty of this work is based on the kinetic studies, which  
84 were divided in two parts. In our opinion, this double fitting contributes also to the  
85 originality of the paper, because the interaction kinetics-radiation becomes clear and is  
86 reflected in the fittings made. This type of studies relating kinetics and radiation, and also  
87 linking it with the predominance of Fenton or photo-Fenton, is not customary and  
88 therefore represents a novelty in this work.

## 89 2. MATERIALS AND EXPERIMENTAL SET-UPS

### 90 2.1. Chemicals and reagents

91 Diphenhydramine hydrochloride was used as a target compound. A concentration of 50  
92 mg/L was chosen to simulate a scenario of wastewaters resulting from pharmaceutical  
93 industries [23] and to assure the monitoring of DPH concentrations in High Performance  
94 Liquid Chromatography (HPLC) and Total Organic Carbon (TOC). Orthophosphoric acid  
95 (Panreac Quimica) and acetonitrile (Fisher Chemical) were employed in (HPLC)  
96 analyses. Hydrogen peroxide was acquired from Merck, and ferrous sulfate ( $\text{FeSO}_4 \cdot$   
97  $7\text{H}_2\text{O}$ ) from Panreac. Ascorbic acid for iron analyses was purchased from Panreac. The

98 initial pH was adjusted with concentrated sulphuric acid (Panreac). Quenching reagents,  
99 such as NaHSO<sub>3</sub> and MeOH, were acquired from Panreac and used to stop the reaction  
100 after sample withdrawal.

## 101 **2.2. Experimental device**

102 The experiments were carried out in a 0.5L Pyrex photoreactor (inner diameter 8 cm,  
103 height 12 cm, supplementary information - Fig. S1), with a magnetic stirrer. 4 LEDs  
104 (Intelligent LED solutions) were located at the top of the reactor. The nominal  
105 consumption of each LED is 1.05 W, operating at 350 mA and with a radiance angle of  
106 125°. The wavelength ranges of the used LEDs were 380-390 and 390-400 nm. The  
107 nitrobenzaldehyde actinometry was performed to determine the incoming radiation in the  
108 UV-LED reactor [24, 25] and the obtained results appear in Fig. 3B. The temperature is  
109 maintained at 25 °C by immersion in a Lauda Alpha thermostatic bath.

## 110 **2.3. Experimental procedure**

111 Degradation of DPH by photo-Fenton was evaluated for one hour, based on previous  
112 experiments [26, 27]. The volume of DPH solution was 0.5L, that means 9 cm of liquid  
113 depth in the photoreactor and 3 cm from the liquid level to the top of photoreactor where  
114 LEDs are located. Different concentrations of H<sub>2</sub>O<sub>2</sub> (25 and 150 mg/L) and Fe<sup>2+</sup> (2.5 and  
115 10 mg/L) were tested. Four previous experiments, for each wavelength range, were done  
116 to determine the optimal concentrations of H<sub>2</sub>O<sub>2</sub> and Fe<sup>2+</sup> (see Fig. 1). These  
117 concentrations of peroxide and iron (10 mg/L Fe<sup>2+</sup> and 150 mg/L H<sub>2</sub>O<sub>2</sub>) were selected to  
118 carry out the rest of the experiments. The pH was adjusted to 2.8 ± 0.2 using H<sub>2</sub>SO<sub>4</sub>. Then,  
119 the FeSO<sub>4</sub>·7H<sub>2</sub>O was introduced in the solution And, finally, H<sub>2</sub>O<sub>2</sub> was added, just before  
120 starting the experiment. During one hour samples were taken at different reaction times  
121 and analyzed. For Fe<sup>2+</sup> quantification, 4 mL of each sample were mixed with 1 mL of

122 buffer solution and 1 mL of o-phenantroline (ISO 6322). At the end of the experiment,  
123 an excess of ascorbic acid was added at each vial to determine the total iron concentration.  
124 The concentration of  $\text{Fe}^{3+}$  was calculated by the difference between the total iron and the  
125  $\text{Fe}^{2+}$  concentration. To quantify the  $\text{H}_2\text{O}_2$  amount, 1.5 mL of each sample were mixed  
126 with 1.5 mL of metavanadate [28], methanol and sodium hydrogen sulfite were employed  
127 to stop the reaction in samples containing  $\text{H}_2\text{O}_2$ . Samples for TOC (15 mL), COD  
128 (Chemical Oxygen Demand) (2.5 mL) and  $\text{UV}_{254}$  (5 mL) were analyzed only at the initial  
129 time and at 60 minutes in each experiment.

#### 130 **2.4. Analytical methods**

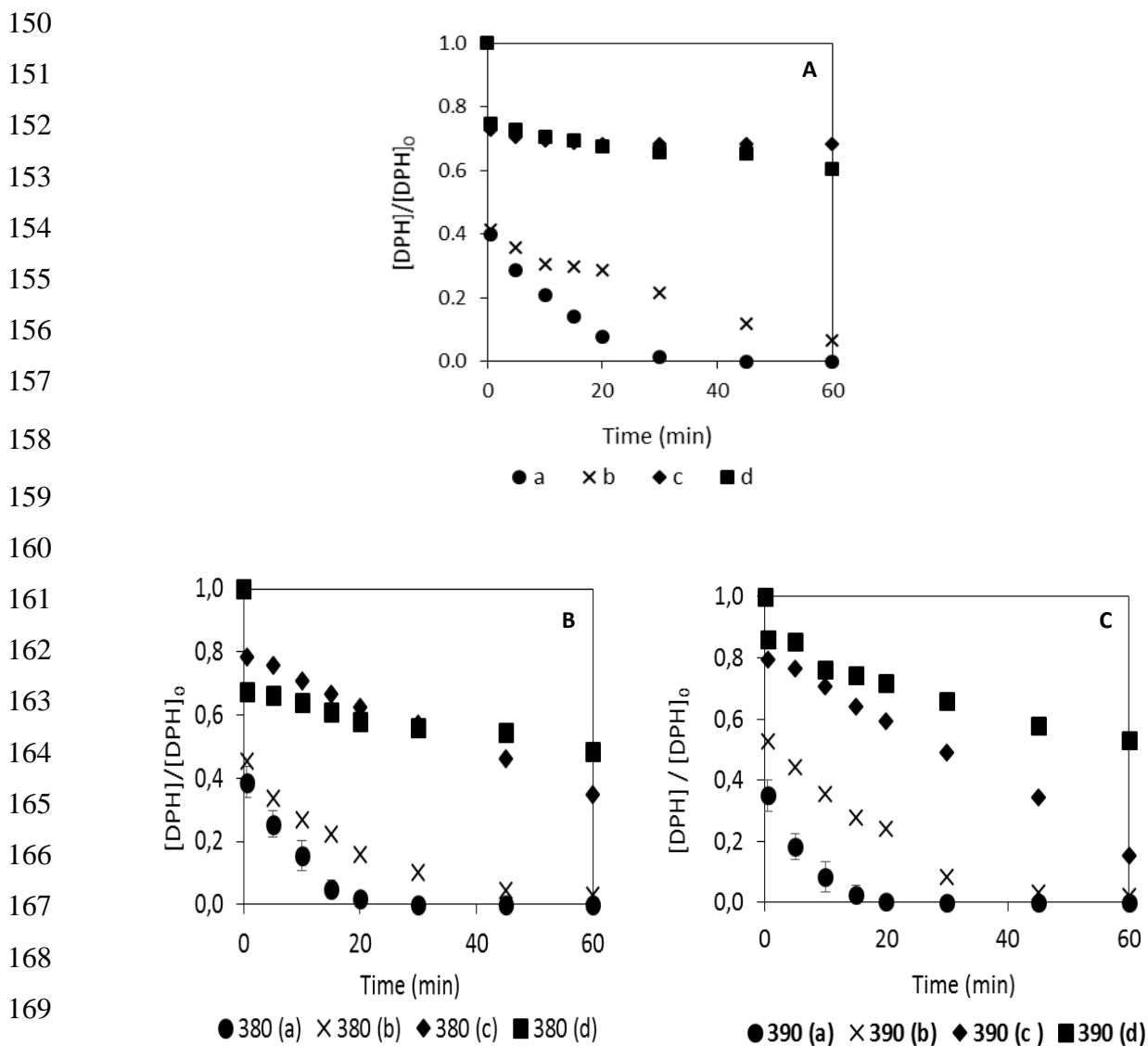
131 DPH was analyzed by an Infinity 1260 HPLC by Agilent with a Teknokroma  
132 Mediterranean Sea 18 column (250 x 4.6 mm i.d; 5 $\mu\text{m}$  particle size). The mobile phases  
133 were acetonitrile (30%) and ultrapure water (70%), adjusted with orthophosphoric acid at  
134 pH=3. A flux of 1.2 mL/min was employed, and the UV detector was set at 220 nm. The  
135 TOC was measured in a Shimadzu TOC-V CNS apparatus. COD was determined  
136 following the Standard Methods [29].  $\text{UV}_{254}$  was analyzed with a HACH DR6000 UV  
137 VIS spectrophotometer. An electrospray ESI-MS and LC/MSD-TOF from Agilent were  
138 employed for the identification of reaction intermediates.

### 139 **3. RESULTS AND DISCUSSIONS**

140 Preliminary tests were performed to study the interaction  $\text{Fe}^{2+}$ -light and  $\text{H}_2\text{O}_2$ -light,  
141 separately. Experiments were carried out with 10 mg/L of  $\text{Fe}^{2+}$  and 150 mg/L of  $\text{H}_2\text{O}_2$ .  
142 Degradation and mineralization were not observed at any tested interaction. Degradation  
143 of DPH by photolysis was also studied and no degradation was observed during 60  
144 minutes.

#### 145 **3.1. Determination of effective concentrations**

146 Figure 1 shows the degradation of DPH with different concentrations of hydrogen  
 147 peroxide and iron II vs. irradiation time. UV-A LEDs emitting in the range 380-400 nm,  
 148 were used. In figure 1A the UV-A LEDs used emit in the range 380-390 nm. However,  
 149 in figure 1B the radiation selected was 390-400 nm.



171 **Figure 1.** DPH degradation by (A) Fenton and (B and C) photo-Fenton process. (B) 380-390 nm. (C) 390-400 nm.  
 172 [DPH] = 50 mg/L. (a) 10 mg Fe<sup>2+</sup>/L - 150 mg H<sub>2</sub>O<sub>2</sub>/L; (b) 10 mg Fe<sup>2+</sup>/L - 25 mg H<sub>2</sub>O<sub>2</sub>/L; (c) 2.5 mg Fe<sup>2+</sup>/L - 150 mg  
 173 H<sub>2</sub>O<sub>2</sub>/L; (d) 2.5 mg Fe<sup>2+</sup>/L - 25 mg H<sub>2</sub>O<sub>2</sub>/L.

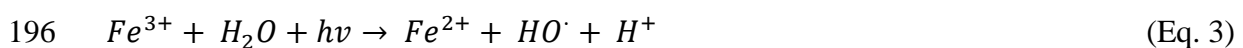
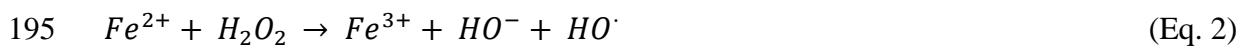
174  
 175 In addition, the accumulated energy ( $Q_{acc}$ , kJ/L) was estimated for each experiment  
 176 according to eq. 1 [30, 31].

177  $Q_{acc} = \sum_{i=0}^n \frac{I \cdot \Delta t_i}{V}$  (Eq.1)

178 I is the incident radiation flow (kJ/s),  $\Delta t_i$  is the increment of the reaction time (s) and V  
 179 stands for the reaction volume (L).

180 Thus, the energy accumulated in each experiment was 0.864 kJ/L (Fig. 1B) and 0.936  
 181 kJ/L (Fig. 1C), at 60 min.

182 The comparison of Figs. 1A and 1B points out that the degradation of DPH is practically  
 183 the same during the first 30 s. This fact indicates that Fenton is the prevailing process,  
 184 according to eq. 2. However, after this initial period (30 s), behavior changes and photo-  
 185 Fenton becomes faster than Fenton. Thus, in the best conditions (10 mg  $Fe^{2+}$ /L and 150  
 186 mg  $H_2O_2$ /L), DPH is totally removed in 30 min with photo-Fenton and 45 min are needed  
 187 to remove completely DPH by Fenton. If the results obtained for the lowest  
 188 concentrations are analyzed (2.5 mg  $Fe^{2+}$ /L and 25 mg  $H_2O_2$ /L), similar results were  
 189 obtained. Thus, the DPH abatement at first 30 seconds with photo-Fenton was 32.4%  
 190 (Fig. 1B) and in the Fenton process was 25.4% (Fig. 1A). Next 30 seconds of the reaction,  
 191 according to eq.3, the  $Fe^{3+}$  is reduced to  $Fe^{2+}$  by UV-A LED, producing more hydroxyl  
 192 radicals, responsible for more DPH removal than in the Fenton process. At 60 minutes  
 193 DPH degradation was 51.6% and 39.4% for photo-Fenton and Fenton, respectively [32,  
 194 33].



198 If the wavelength range influence is considered (Fig. 1B and 1C), it can be observed that  
 199 time for total DPH removal is the same in both cases (30 min) for the best conditions (10



200 mg Fe<sup>2+</sup>/L and 150 mg H<sub>2</sub>O<sub>2</sub>/L). The DPH removal is also similar (97.0%, for 380-390  
201 nm, and 97.9%, for 390-400 nm, at 60 min) when 10 mg Fe<sup>2+</sup>/L and 25 mg H<sub>2</sub>O<sub>2</sub>/L were  
202 used. However, for the rest of Fe<sup>2+</sup> and H<sub>2</sub>O<sub>2</sub> concentrations tested, the shape of the  
203 graphics is close but values are a little different. Thus, the final degradation of DPH (60  
204 min) was similar in both wavelength ranges tested for 2.5 mg Fe<sup>2+</sup>/L and 25 mg H<sub>2</sub>O<sub>2</sub>/L,  
205 being 51.6% and 46.9% for 380-390 nm and 390-400 nm, respectively. Differences  
206 increase for concentrations of 25 mg Fe<sup>2+</sup>/L and 150 mg H<sub>2</sub>O<sub>2</sub>/L, being DPH removal, at  
207 60 min, 65.1% for 380-390 nm and 84.8% for 390-400 nm. These differences can be  
208 explained because radiation and hydrogen peroxide concentration play more important  
209 role in the second part of the process, after the initial 30 s, where photo-Fenton (reaction  
210 3) prevails.

211 If the last values (2.5 mg Fe<sup>2+</sup>/L and 25/150 mg H<sub>2</sub>O<sub>2</sub>/L) are compared with Fenton process  
212 (fig. 1A), as commented before, large differences were observed because in Fenton  
213 process, after the initial 30s, the degradation rate decreases dramatically compared to the  
214 photo-Fenton process (fig. 1B and 1C). This fact points out again the important role-  
215 played by the light.

216 Summarizing, from these results it seems that Fe<sup>2+</sup> plays an important role at the initial  
217 moments of the experiment (30 s) and reaction 2 prevails, that means Fenton is the  
218 predominant process and a little synergistic effect of photo-Fenton can aid to DPH  
219 degradation. On the contrary, H<sub>2</sub>O<sub>2</sub> concentration and light acquire the predominant role  
220 during the rest of the experiment, meaning that photo-Fenton prevails (reactions 3 and 4).  
221 Moreover, from the shape of graphics presented in Fig. 1, it seems that the influence of

222  $\text{Fe}^{2+}$  concentration on the degradation of DPH is higher than the influence of  $\text{H}_2\text{O}_2$   
 223 concentration.

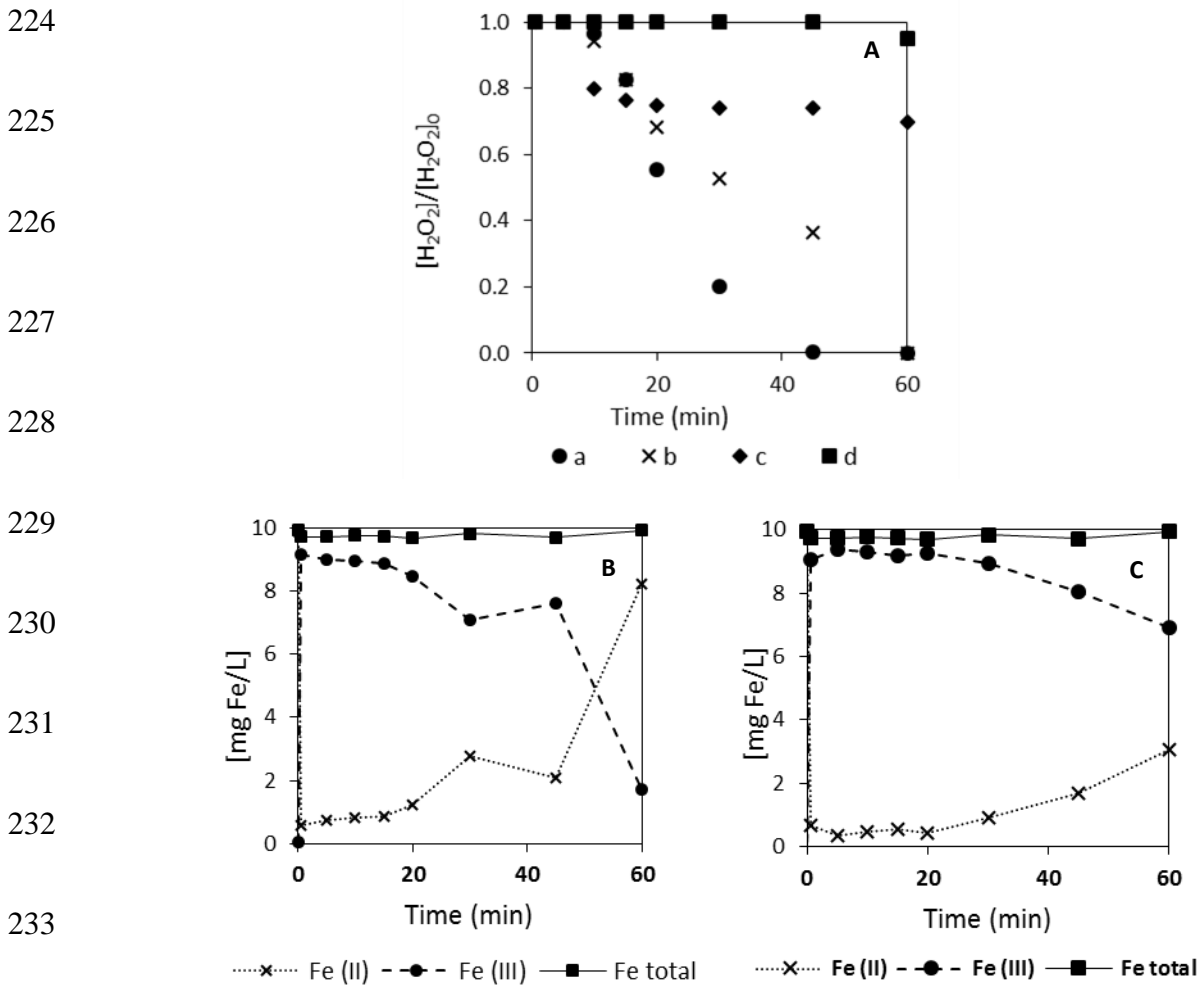


**Figure 2.** (A) Hydrogen peroxide consumption in photo-Fenton process. (a)  $10 \text{ mgFe}^{2+}/\text{L} - 150 \text{ mg H}_2\text{O}_2/\text{L}$ ; (b)  $10 \text{ mgFe}^{2+}/\text{L} - 25 \text{ mg H}_2\text{O}_2/\text{L}$ ; (c)  $2.5 \text{ mgFe}^{2+}/\text{L} - 150 \text{ mg H}_2\text{O}_2/\text{L}$ ; (d)  $2.5 \text{ mgFe}^{2+}/\text{L} - 25 \text{ mg H}_2\text{O}_2/\text{L}$ . (B) Species of iron vs. irradiation time. ((a)  $10 \text{ mg Fe}^{2+}/\text{L}$  and  $150 \text{ mg H}_2\text{O}_2/\text{L}$ ; (b)  $10 \text{ mg Fe}^{2+}/\text{L}$  and  $25 \text{ mg H}_2\text{O}_2/\text{L}$ ). The lines show an experimental decay fit and are presented only to appreciate better

237 The consumption of hydrogen peroxide confirms all that explained in the previous  
 238 paragraphs (see Fig. 2A). As expected, the  $\text{H}_2\text{O}_2$  consumption increased with the iron and  
 239 hydrogen peroxide concentrations. Thus, for the same concentration of iron (II), when the  
 240 concentration of hydrogen peroxide increases, its consumption also increases, according

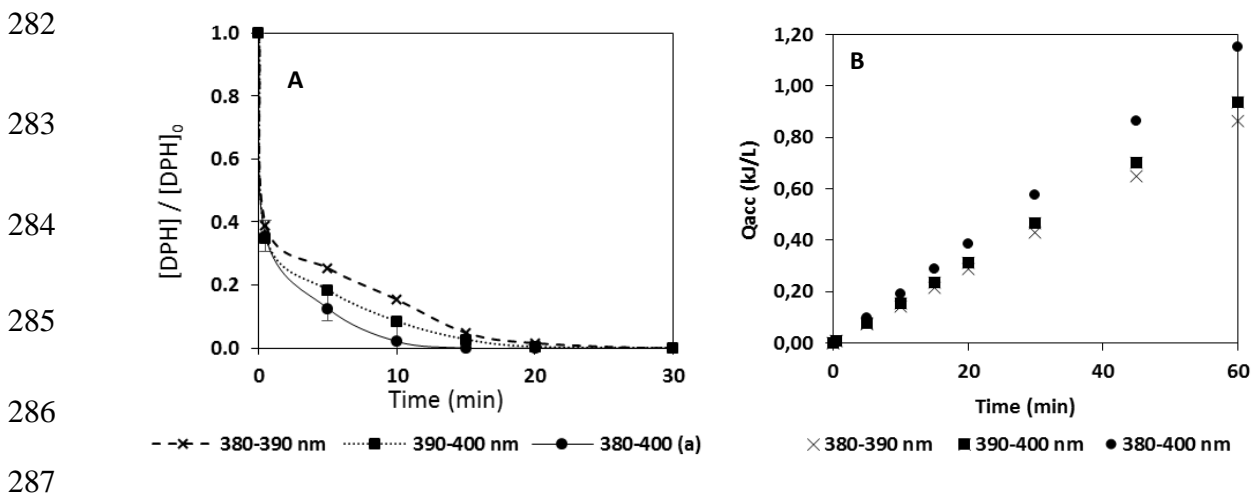
241 to Eq. 2 and Eq. 4. It has also to be said that the same trend was observed in the  
242 experiments made in the range 380-390 nm.

243 Iron evolution was also followed (see Fig. 2B and Fig. 2C). The first observation was that  
244 total iron ( $Fe_{tot}$ ) remained constant during the experiment. For 10 mg  $Fe^{2+}/L$  and 150 mg  
245  $H_2O_2/L$  (molar ratio  $H_2O_2:Fe^{2+} = 25$ ), at the first minute, all ferrous iron was almost  
246 oxidized to ferric iron. Thus,  $Fe^{2+}$  reacts quickly with the hydrogen peroxide to give  
247 hydroxyl radicals in large quantity, according to the eq. 2 and as explained in section 3.1.  
248 This behavior would explain the fast decrease in DPH concentration observed during the  
249 first 30 seconds and confirms that Fenton prevails at these initial moments of the  
250 experiment (eq. 2), as commented before. After that, the  $Fe^{3+}$  was reduced to  $Fe^{2+}$  step by  
251 step in the course of the experiment. The eq. 3 begins to take place and the photo-Fenton  
252 process begins to act. However, for 10 mg  $Fe^{2+}/L$  and 25 mg  $H_2O_2/L$  (molar ratio  
253  $H_2O_2:Fe^{2+} = 4$ ), lower iron regeneration was seen, because the excess of hydrogen  
254 peroxide is lower and the regeneration of  $Fe^{2+}$ , from  $Fe^{3+}$  (eq.4) is more difficult. A proper  
255 ratio between iron (II) and hydrogen peroxide concentrations is fundamental to maximize  
256 the  $HO\cdot$  production and thus the good performance of the oxidation process. The  
257 generation of hydroxyl radicals is higher when concentration of  $H_2O_2$  and Fe (II) are  
258 higher, as commented above [34, 35]. However, to avoid scavenging effects due to excess  
259 amounts of  $H_2O_2$  (because hydroxyl radical can also react with  $H_2O_2$ ), selecting an  
260 optimal dose of this reagent is important. The needed concentrations of the reagents ( $H_2O_2$   
261 and Fe(II)), in turn, depend on the effluent characteristics [36]. Rodríguez-Chueca and  
262 coworkers [37], for instance, studied the effect of  $H_2O_2/Fe^{2+}$  ratio on COD removal and  
263 the results revealed that a ratio of approximately 31 (5,500 mg/L of  $H_2O_2$  and 180 mg/L  
264 of  $Fe^{3+}$ ) gave the best results (achieving 42.05% of COD removal in 180 min). For the  
265 same concentration of iron (III) but less concentration of  $H_2O_2$  (1100 mg/L) (ratio

266  $\text{H}_2\text{O}_2/\text{Fe}^{3+} = 6$  approx.) the result of COD removal at the same time was lower (23.35%).  
 267 These results are in accordance with this study. When 10 mg  $\text{Fe}^{2+}/\text{L}$  and 150 mg  $\text{H}_2\text{O}_2/\text{L}$   
 268 (which implies the highest  $\text{H}_2\text{O}_2/\text{Fe}^{2+}$  ratio and high concentrations of  $\text{H}_2\text{O}_2$  and Fe (II)),  
 269 were tested, high removal of DPH was achieved. The optimal relationship between COD  
 270 removal and oxidant dosage has also been studied. An increase in  $\text{H}_2\text{O}_2/\text{COD}$  weight ratio  
 271 favors an enhancement in micropollutants degradation [38]. Bolobajev and coworkers  
 272 [38], among others, studied this aspect of the process. The results revealed that a higher  
 273 ratio, which means more  $\text{H}_2\text{O}_2$  per unit of COD, leads to the best performance in terms of  
 274 organic matter degradation. Like the  $\text{Fe}^{2+}/\text{H}_2\text{O}_2$  ratio, the  $\text{H}_2\text{O}_2/\text{COD}$  optimal ratio  
 275 depends on a large extent on the characteristics of the effluent [39]. Again, these results  
 276 are in accordance with the observations in this study.

### 277 3.2. Synergistic effects of two wavelengths combination

278 Figure 3A shows the influence of the wavelength range on the DPH degradation for 10  
 279 mg  $\text{Fe}^{2+}/\text{L}$  and 150 mg  $\text{H}_2\text{O}_2/\text{L}$ . Two wavelengths were tested (380-390 nm and 390-400  
 280 nm) and the combination of both LEDs (380-400 nm). The nominal power in all  
 281 experiments was 4.2 W.



288 **Figure 3.** (A) DPH degradation by photo-Fenton and (B) radiation accumulation with different LEDs wavelengths  
 289  $[\text{DPH}]_0 = 50 \text{ mg/L}$ ;  $[\text{Fe}^{2+}] = 10 \text{ mg/L}$ ;  $[\text{H}_2\text{O}_2] = 150 \text{ mg/L}$ ; Nominal power = 4.2 W.

290 As it can be observed in Fig. 3A, from the use of radiation of 380-390 nm (0.432 kJ/L) or  
291 390-400 nm (0.468 kJ/L) does not imply a significant increase regarding total DPH  
292 removal, which is achieved at 30 min in both cases. However, there are little differences  
293 in the DPH degradation curve until 20 minutes and range 390-400 nm presents a faster  
294 degradation, because the accumulated radiation is always a little higher in the range 390-  
295 400 nm.

296 When two wavelengths were combined (15 min,  $Q_{acc}= 0.288$  kJ/L, 380-400 nm), the  
297 degradation of DPH was 100% in only 15 minutes (the degradation time is reduced by  
298 half), due to the synergistic effect of the two wavelengths working jointly that increases  
299 the efficiency of the process. This rise of DPH degradation, for 380-390 and 390-400 nm,  
300 is logical according the accumulated energy. As it can be observed in Fig. 3B, the  
301 accumulated energy was higher than this one corresponding to the two wavelengths acting  
302 separately at any time.

303 The increase in efficiency was also reflected in AOS (Eq. 5), COD and TOC, and the  
304 highest values for these parameters were obtained for 380-400 nm (see Table 1). More  
305 explanations about this behavior can be found at the end of section 3.3.

### 306 **3.3. Kinetics, synergies and radiation**

307 The experimental data shown in Fig. 1 were fitted to a pseudo-first order kinetics,  
308 according to eq. 6.

$$309 \ln\left(\frac{C_{DPH}}{C_{DPH0}}\right) = k' \cdot t \quad (\text{Eq. 6})$$

310 Where  $C_{DPH0}$  is the initial DPH concentration (mg/L),  $C_{DPH}$  is the final DPH concentration  
311 (mg/L),  $t$  is the time (min) and  $k$  is an apparent reaction rate constant ( $\text{min}^{-1}$ ). From the  
312 plot of  $\ln(C_{DPH}/C_{DPH0})$  vs. time, the kinetics were obtained for each experimental

313 conditions. However, looking at Fig. 1, two zones can be clearly seen for all experiments.  
314 In the initial moments, up to 30 seconds, a very fast decrease in the concentration of DPH  
315 can be seen. After 30 seconds, the decrease is much smoother. Therefore, the fitting has  
316 also been divided into two parts. In the first 30 seconds, the initial reaction rate method  
317 is used to calculate the kinetic constant, assuming order 1. From there, the rest of the data  
318 to the end of the experiment were fitted to pseudo-first order kinetics. The final time was  
319 60 minutes for all cases, except for 10 mg Fe<sup>2+</sup>/L and 150 mg H<sub>2</sub>O<sub>2</sub>/L, where final time  
320 was 30 minutes due to DPH was totally removed at this time. The results obtained in the  
321 fittings are shown in Table 1. In addition, the fitting of data from Fig. 1 to pseudo-first  
322 order kinetics is shown in Figure S2 (supplementary information), for reaction times  
323 higher than 30 seconds.

324 Average Oxidation State (AOS), COD and TOC were also analyzed. Table 1 summarizes  
325 the obtained results. The calculation of AOS was performed according to Eq. 5, where  
326 TOC and COD are represented in mol/L of C and O<sub>2</sub>, respectively. As known, this  
327 indicator takes values between +4 (value for CO<sub>2</sub>), state of maximum oxidation of carbon,  
328 and -4 (value for CH<sub>4</sub>), state of maximum reduction [30].

$$329 \quad AOS = 4 \times \frac{TOC - COD}{TOC} \quad (\text{Eq. 5})$$

330 AOS started at a value of 1.0 (at initial time) and increased to the highest values using the  
331 highest concentrations of iron II and peroxide. The same trend was found in COD and  
332 TOC. A high degree of mineralization (54.2%) and oxidation (79.9%) were observed at  
333 60 minutes, for the highest concentrations of peroxide and iron II. At this time, DPH has  
334 been completely degraded. This signified a rising oxidation and break of the DPH leading  
335 to more oxidized molecules. However, for 2.5 mg Fe<sup>2+</sup>/L and 25 mg H<sub>2</sub>O<sub>2</sub>/L  
336 mineralization and oxidation were not observed. These results show again that both the

337 hydrogen peroxide and iron (II) concentrations play an important role in the photo-Fenton  
 338 process.

339 **Table 1.** Values of the kinetic constants for different wavelengths and concentrations of Fe<sup>2+</sup> and H<sub>2</sub>O<sub>2</sub>. k<sub>1</sub> is the kinetic  
 340 constant obtained during the first 30 seconds and k<sub>2</sub> is the kinetic constant for the rest of the experiment (fitting to  
 341 pseudo first order kinetics)

Wavelength (nm)	[Fe <sup>2+</sup> ] (mg/L)	[H <sub>2</sub> O <sub>2</sub> ] (mg/L)	k <sub>1</sub> (min <sup>-1</sup> )	k <sub>2</sub> (min <sup>-1</sup> )	R <sup>2</sup> k <sub>2</sub>	AOS	COD (%)	TOC (%)
380-390	10	150	1.9	0.16	0.96	2.4	70.2	54.2
380-390	10	25	1.6	0.05	0.99	1.2	14.4	6.8
380-390	2.5	150	0.5	0.01	0.99	1.0	6.6	2.8
380-390	2.5	25	-	0.005	0.96	N/A	0.0	0.0
390-400	10	150	2.1	0.23	0.95	2.7	79.9	60.5
390-400	10	25	1.3	0.06	0.98	1.3	15.2	6.9
390-400	2.5	150	0.5	0.03	0.93	1.0	6.7	2.9
390-400	2.5	25	0.3	0.008	0.98	N/A	0.0	0.0
380-400	10	150	2.1	0.3	0.99	3.8	95.6	70.1

342

343 From the data of Table 1, it is observed that the best results are obtained for 10 mg Fe<sup>2+</sup>/L  
 344 and 150 mg H<sub>2</sub>O<sub>2</sub>/L, for all the wavelength ranges tested.

345 Concerning the values of k<sub>1</sub>, the wavelength of the radiation used does not have much  
 346 influence. For instance, k<sub>1</sub> value is 0.5 min<sup>-1</sup> for 380-390 nm and 390-400 nm, for 2.5 mg  
 347 Fe<sup>2+</sup>/L and 150 mg H<sub>2</sub>O<sub>2</sub>/L. However, data show that iron and peroxide concentrations  
 348 have large influence on the reaction rate. As an example, k<sub>1</sub> values are 2.1 min<sup>-1</sup>, for 10  
 349 mg Fe<sup>2+</sup>/L and 150 mg H<sub>2</sub>O<sub>2</sub>/L, and 0.3 min<sup>-1</sup>, for 2.5 mg Fe<sup>2+</sup>/L and 25 mg H<sub>2</sub>O<sub>2</sub>/L, in

350 the range 390-400 nm. Results of Table 1 for  $k_1$  confirm also that the concentration of  
351  $\text{Fe}^{2+}$  has a higher influence than the concentration of  $\text{H}_2\text{O}_2$ .

352 Once the initial moments (30 s) have passed, it can be observed a similar behavior of the  
353 system concerning the influence of  $\text{Fe}^{2+}$  and peroxide concentrations on the reaction rate.  
354 Thus, the highest values of  $k_2$  are obtained for the concentrations of 10 mg  $\text{Fe}^{2+}/\text{L}$  and  
355 150 mg  $\text{H}_2\text{O}_2/\text{L}$ . This behavior appears as logical because  $\text{Fe}^{3+}$  slowly returns to  $\text{Fe}^{2+}$  and,  
356 therefore, the generation of hydroxyl radicals through the eq. 3 is slower (see Fig. 3B). In  
357 addition, it seems that the wavelength can play a role, because, for the same concentration  
358 of iron and peroxide,  $k_2$  is higher always for the experiments in the range 390-400 nm.

359 Comparing  $k_1$  and  $k_2$  values, it can be seen that  $k_2$  is one order of magnitude lower than  
360  $k_1$  for all the tested concentrations of  $\text{Fe}^{2+}$  and peroxide and for all the wavelength ranges.  
361 This fact can be due to several factors and, among them, it could be mentioned that, after  
362 the initial instants, intermediates appear which compete with DPH for hydroxyl radicals.  
363 Hence, the degradation of DPH slows down. These results are in accordance with eq.2, 3  
364 and 4 if the reactions rates are considered. The reaction rate corresponding to eq.2 is 63  
365  $\text{M}^{-1} \text{s}^{-1}$ . However, the value for eq. 4 is lower than eq.2 ( $10^{-3}$ - $10^{-2} \text{M}^{-1} \text{s}^{-1}$ ) [40].

366 In order to study the synergy of wavelengths, as explained before, experiments were made  
367 using 4 LEDs at the top of the reactor, like explained just now, but in this case, 2 LEDs  
368 with 380-390 nm and 2 LEDs with 390-400 nm were combined. Experiments were done  
369 only for the best conditions (10 mg  $\text{Fe}^{2+}/\text{L}$  and 150 mg  $\text{H}_2\text{O}_2/\text{L}$ ). As has been done when  
370 the two wavelength ranges were studied separately, the experimental data are fitted for  
371 two different periods of time: during the initial moments (up to 30 s) and from there to  
372 the end of the experiment. For the initial time (first 30 s), the value of the kinetic constant  
373 ( $k_1$ ) was  $2.1 \text{ min}^{-1}$  (see Table 1). This value is very close to the values obtained for  $k_1$



374 when LEDs of 380-390 nm or LEDs of 390-400 nm were used. As commented before,  
375 the reaction at this initial moment is very fast and it is strongly related to the  $\text{Fe}^{2+}$   
376 concentration. It can be said that the generation of hydroxyl radicals is practically due to  
377  $\text{Fe}^{2+}$  oxidation (eq. 2), meaning that the role of radiation is not so important (Fenton  
378 process). Thus, wavelength has not a large influence.

379 After the initial 30 s, the kinetic constant ( $k_2$ ) obtained with the combined LEDs was 0.3  
380  $\text{min}^{-1}$  which is practically one order of magnitude lower than  $k_1$ , as occurs with 380-390  
381 nm and 390-400 nm studied separately (see Table 1). This  $k_2$  value of  $0.3 \text{ min}^{-1}$  is higher  
382 than  $k_2$  values obtained for the LEDs of 380-390 nm or 390-400 nm (see also Table 1)  
383 because, after the first 30s, the reaction of  $\text{Fe}^{3+}$  reduction with  $\text{H}_2\text{O}_2$  and light (eq. 3) is  
384 more important and photo-Fenton process is acting. This means that the role of the  
385 radiation is important after the initial period of 30 s, and explains that wavelength used  
386 has more influence. In addition, the effect of synergy could be explained from Eq. 7.

$$387 \quad r = \sum_{\lambda} \varphi_{\lambda} \cdot \mu_{\lambda} \cdot I_{\lambda} \quad (\text{Eq. 7})$$

388 Where  $r$  is the reaction rate ( $\text{mol} \cdot \text{cm}^{-3} \cdot \text{s}^{-1}$ ),  $\varphi_{\lambda}$  is the quantum yield ( $\text{mol}/\text{Einstein}$ ),  $\mu_{\lambda}$  is  
389 the absorbance ( $\text{cm}^{-1}$ ) and  $I_{\lambda}$  is the photonic flow ( $\text{Einstein} \cdot \text{cm}^{-2} \cdot \text{s}^{-1}$ ). According to eq. 7,  
390 the reaction rate in any photochemical process depends on the absorbance, quantum yield  
391 and radiation intensity. These parameters can be considered a little different in the range  
392 of 380-390 nm or in the range 390-400 nm. For this reason, the results obtained for  $k_2$  can  
393 change a little in these two ranges (see Table 1). In the range 380-400 nm, considering  
394 that  $r$  is the summation for all the wavelengths range (see eq. 6), it seems logical to expect  
395 that reaction rate increases. This is that we have observed experimentally and can explain  
396 that  $k_2$  for the range 380-400 nm is higher than  $k_2$  for the range 380-390 nm or for the  
397 range 390-400 nm. In fact, the consideration of  $k_2/Q_{\text{acc}}$  for each range of wavelength prove

398 the synergy explained above. This calculation was done for 30 minutes (380-390 and 390-  
 399 400 nm) and 15 minutes (380-400 nm), time at DPH was total removed. Values of 0.37,  
 400 0.49 and 1.04 correspond at 380-390, 390-400 and 380-400 nm. Thus, it is clear that 380-  
 401 400 nm presents a value much higher confirming the synergistic effect of wavelength  
 402 according to eq. 7.

### 403 3.4. By-products and degradation pathways

404 As explained in section 2, the intermediates of DPH were detected by LC/MS during the  
 405 photo-Fenton process. Four intermediates were identified at the final of each experiment  
 406 (60 minutes):  $C_{17}H_{23}NO_5$ ,  $C_{17}H_{21}NO_3$ ,  $C_{17}H_{21}NO_2$  and  $C_{13}H_{10}O$  (see table S1 in  
 407 supplementary material). Fig. 4 presents the evolution of the intermediates during one  
 408 hour in different scenarios.

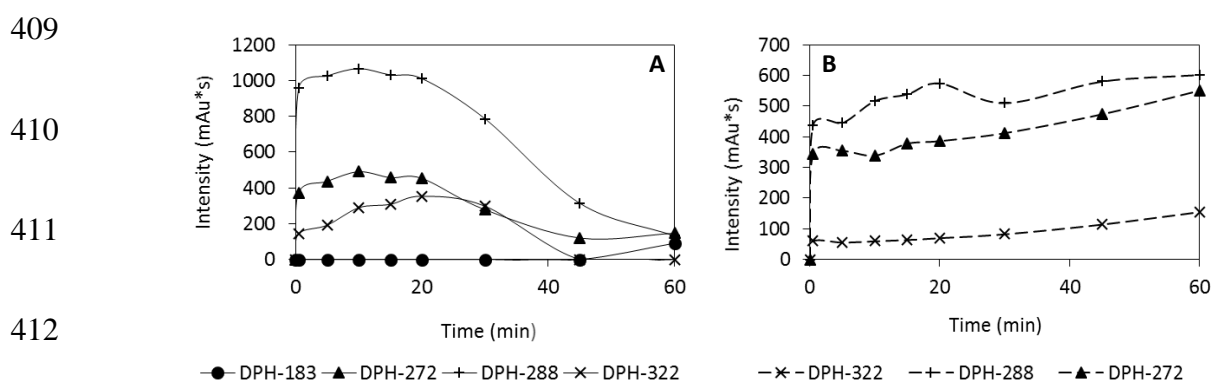


**Figure 4.** Evolution of intermediates identified in different scenarios during the experiment.  $[DPH]_0 = 50$  mg/L; Nominal power: 4.2W. A) 10 mg  $Fe^{2+}/L$  and 150 mg  $H_2O_2/L$ ; B) 2.5 mg  $Fe^{2+}/L$  and 25 mg  $H_2O_2/L$ .

413 Fig. 4A and Fig. 4B, represent intermediates identified in the best and the worst conditions  
 414 regarding concentrations of iron (II) and hydrogen peroxide. The wavelength range used  
 415 was 390-400 nm, but the same trend was observed for 380-390 nm and 380-400 nm.  
 416 When 10 mg  $Fe^{2+}/L$  and 150 mg  $H_2O_2/L$  were tested, the intermediates began to degrade  
 417 at approximately 15 minutes. This time corresponds to the moment when there is a low  
 418 concentration of DPH. In addition, DPH-183 was formed at 60 minutes due to the higher

419 formation of hydroxyl radicals. This fact allows the degradation almost entirely of the  
420 first intermediates and formation of more oxidized intermediates.

421 However, when 2.5 mg Fe<sup>2+</sup>/L and 25 mg H<sub>2</sub>O<sub>2</sub>/L were tested, the intermediates formed  
422 did not degrade because DPH degradation reaction is not so fast (46.9% removal at 60  
423 minutes). This means that the hydroxyl radicals are still mainly engaged in attacking the  
424 DPH. Thus, at 60 minutes the concentration of formed intermediates was higher than at  
425 the initial time because the intermediates have not yet begun to degrade. In addition, the  
426 intermediate DPH-183 does not appear because it comes from the degradation of DPH-  
427 272 (see Fig. S3) which has not started yet after 60 minutes of reaction (see Fig. 4B). It  
428 can be concluded that, as expected, the initial concentration of Fe<sup>2+</sup> and H<sub>2</sub>O<sub>2</sub> have a large  
429 influence on DPH degradation and, as a consequence, of the intermediates formation and  
430 degradation. Thus, the highest concentrations of Fe<sup>2+</sup> and H<sub>2</sub>O<sub>2</sub> give the fastest formation  
431 and degradation of intermediates (see Fig. 4A).

432 Figure S3 (supplementary material) presents a proposed DPH degradation pathway with  
433 the intermediates found. DPH-272, DPH-288 and DPH-322 could be formed from  
434 primary oxidation of the parent compound (DPH-256). The generation of DPH-272  
435 appears to be due to the hydroxylation of the initial compound. DPH-322 might be formed  
436 by the opening of an aromatic ring in DPH-256. In addition, the hydroxylation and  
437 oxidation of one carbon from the initial compound could have led to the generation of  
438 DPH-288. Finally, DPH-183 could be produced by consecutive  
439 deamination/dihydroxylation reactions taking place in the DPH-272 structure.

#### 440 **4. CONCLUSIONS**

441 UVA-LEDs (380-390 nm and 390-400 nm) are useful for DPH degradation. In addition,  
442 the combination of LEDs with 380-390 nm and 390-400 nm wavelength ranges produces  
443 synergistic effects on DPH removal.

444 The best results in DPH degradation were obtained for the highest concentrations of iron  
445 and peroxide (10 mg Fe<sup>2+</sup>/L and 150 mg H<sub>2</sub>O<sub>2</sub>/L).

446 Kinetic studies pointed out that the initial reaction rate (up to 30 s) is higher than the rate  
447 during the rest of the experiment, showing the influence of Fe<sup>2+</sup> concentration. Thus,  
448 Fenton process prevails at the initial moments and photo-Fenton during the rest of the  
449 experiment.

450 Three intermediates (DPH-272, DPH-288 and DPH-322) were generated from the  
451 oxidation of initial compound and DPH-188 was produced by subsequent reactions from  
452 DPH-272.

#### 453 **Acknowledgments**

454 The authors are appreciative of the financing acquired by the Ministry of Science and  
455 Innovation of Spain (projects CTQ2014-52607-R and CTQ2017-86466-R), Ministry of  
456 Education, Culture and Sports (FPU research fellowship FPU-16/02101), Institute for  
457 Water Research (IdRA) of Universitat de Barcelona and AGAUR-Generalitat de  
458 Catalunya (project 20145GR245 and 2017SGR-131).

#### 459 **References**

460 [1] P. Verlicchi, A. Galletti, M. Petrovic, D. Barceló, Hospital effluents as a source of  
461 emerging pollutants: an overview of micropollutants and sustainable treatment options,  
462 Journal of Hydrology 389 (2010) 416-428.

463 [2] W. Gebhardt, H.F. Schroder, Liquid chromatography-(tandem) mass spectrometry for  
464 the follow-up of the elimination of persistent pharmaceuticals during wastewater  
465 treatment and advanced oxidation, *Journal of Chromatography A* 1160 (2007) 34-43.

466 [3] R.P. Deo, Pharmaceuticals in the surface water of the USA: A review, *Current*  
467 *Environmental Health Reports* 1 (2014) 113-122. *Journal of Hazardous Materials* 148  
468 (2007) 751-755.

469 [4] C. Comninellis, A. Kapalka, S. Malato, S.A. Parsons, I. Poulios, D. Mantzavinos,  
470 Advanced Oxidation Processes for water treatment: advances and trends for R&D,  
471 *Journal of Chemical Technology and Biotechnology* 83 (2008) 769-776.

472 [5] J. Kumar, A. Bansal, Photocatalysis by Nanoparticles of Titanium Dioxide for  
473 Drinking Water Purification: A Conceptual and State-of Art Review, *Materials Science*  
474 *Forum* 764 (2013) 130-150.

475 [6] A.V. Wankhade, G.S. Gaikwad, M.G. Dhonde, N.T. Khat, S.R. Thakare, Removal of  
476 organic pollutant from water by heterogeneous photocatalysis: a review, *Research Journal*  
477 *of Chemistry and Environmental* 17 (2013) 84-94.

478 [7] O. Primo, M.J. Rivero, I. Ortiz, Photo-Fenton process as an efficient alternative to the  
479 treatment landfill leachates, *Journal of Hazardous Materials* 153 (2008) 834-842.

480 [8] O. Primo, A. Rueda, M.J. Rivero, I. Ortiz, An integrated process, Fenton reaction-  
481 ultrafiltration, for the treatment of landfill leachate: Pilot plant operation and analysis,  
482 *Industrial & Engineering Chemistry Research* 47 (2008) 946-952.

483 [9] S.Y. Lee, S.J. Park, TiO<sub>2</sub> photocatalyst for water treatment applications, *Journal of*  
484 *Industrial & Engineering Chemistry* 19 (2013) 1761-1769.

- 485 [10] J.J. Pignatello, A. MacKay, Advanced oxidation processes for organic contaminant  
486 destruction based on the Fenton reaction and related chemistry, *Critical Reviews in*  
487 *Environmental Science and Technology* 36 (2006) 1-84.
- 488 [11] I. Carra, J.A. Sánchez Pérez, S. Malato, O. Autin, B. Jefferson, P. Jarvis, Application  
489 of high intensity UVC-LED for the removal of acetamiprid with the photo-Fenton  
490 process, *Chemical Engineering Journal* 264 (2015) 690-696.
- 491 [12] O. Autin, C. Romelot, L. Rust, J. Hart, P. Jarvis, J. MacAdam, S.A. Parsons, B.  
492 Jefferson, Evaluation of a UV-light emitting diodes unit for the removal of  
493 micropollutants in water for low energy advanced oxidation processes, *Chemosphere* 92  
494 (2013) 745-751.
- 495 [13] P. Xiong, J. Hu, Degradation of acetaminophen by UVA/LED/TiO<sub>2</sub> process,  
496 *Separation and Purification Technology* 91 (2012) 89-95.
- 497 [14] S. Verma, M. Sillanpää, Degradation of anatoxin-a by UV-C LED and UV-C  
498 LED/H<sub>2</sub>O<sub>2</sub> advanced oxidation processes, *Chemical Engineering Journal* 274 (2015) 274-  
499 281.
- 500 [15] R.J. Tayade, T.S. Natarajan, H.C. Bajaj, Photocatalytic degradation of methylene  
501 blue dye using ultraviolet light emitting diodes, *Industrial & Engineering Chemistry*  
502 *Research* 48 (2009) 10262-10267.
- 503 [16] M.A. Würtele, T. Kolbe, M. Lipsz, A. Külberg, M. Weyers, M. Kneissl, M. Jekel,  
504 Application of GaN-based ultraviolet-C light emitting diodes-UV-LEDs-for water  
505 disinfection, *Water Research* 45 (2011) 1481-1489.

506 [17] G. Matafonova, V. Batoev, Recent advanced in application of UV light-emitting  
507 diodes for degrading organic pollutants in water through advanced oxidation processes:  
508 A review, *Water Research* 132 (2018) 177-189.

509 [18] I. De la Odra, B. Esteban García, J.L. García Sánchez, J.L. Casas López, J.A.  
510 Sánchez Pérez, Low cost UVA-LED as a radiation source for the photo-Fenton process:  
511 a new approach for micropollutant removal from urban wastewater, *Photochemical &*  
512 *Photobiological Sciences* 16 (2017) 72-78.

513 [19] A.C. Chevremont, A.M. Farnet, M. Sergent, B. Columb, Effect of coupled UV-A  
514 and UV-C LEDs on both microbiological and chemical pollution of urban wastewaters,  
515 *Science of Total Environment* 426 (2012) 304-310.

516 [20] N.F.F. Moreira, J.M. Sousa, G. Macebo, A.T. Ribeiro, L. Barrientos, M. Pedrosa,  
517 J.L. Faria, F.R. Pereira, S. Castro-Silva, M.A. Segundo, C.M. Manaia, O.C. Nunes,  
518 A.M.T. Silva, Photocatalytic ozonation of urban wastewater and surface water using  
519 immobilized TiO<sub>2</sub> with LEDs: Micropollutants, antibiotic resistance genes and estrogenic  
520 activity, *Water Research* 94 (2016) 10-22.

521 [21] M.H. Rasoulifard, M. Fazli, M.R. Eskandarian, Performance of the light-emittind  
522 diodes in a continuous photoreactor for degradation of Direct Red using UV-LED/S<sub>2</sub>O<sub>8</sub><sup>2-</sup>  
523 process, *Journal of Industrial & Engineering Chemistry* 24 (2015) 121-126.

524 [22] K. Hölz, J. Lietard, M.M. Somoza, High-Power 365 nm UV LED mercury Arc Lamp  
525 replacement for photochemistry and chemical photolithography, *AC Sustainable*  
526 *Chemistry & Engineering* 5 (2017) 828-834.

527 [23] D.G. Joakim Larrson, C. De Pedro, N. Paxeus, Effluent from drug manufactures  
528 contains extremely high levels of pharmaceuticals, *Journal of Hazardous Materials* 148  
529 (2007) 751-755.

530 [24] H.J. Kuhn, S.E. Braslavsky, R. Schmidt, Chemical actinometry (IUPAC Technical  
531 Report), Pure Applied Chemistry 76 (2004) 2105-2146.

532 [25] E.S. Galbavy, K. Ram, C. Anastasio, 2-Nitrobenzaldehyde as a chemical actinometer  
533 for solution and ice photochemistry, Journal of Photochemistry and Photobiology A:  
534 Chemistry 209 (2010) 186-192.

535 [26] N. López, S. Plaza, A. Afkhami, P. Marco, J. Giménez, S. Esplugas, Treatment of  
536 Diphenhydramine with different AOPs including photo-Fenton at circumneutral pH,  
537 Chemical Engineering Journal 318 (2017) 112-120.

538 [27] N. López, P. Marco, J. Giménez, S. Esplugas, Photocatalytic diphenhydramine  
539 degradation under different radiation sources: Kinetic studies and energetic comparison,  
540 Applied Catalysis B: Environmental 220 (2018) 497-505.

541 [28] R.F. Pupo Nogueira, M.C. Oliveira, W.C. Paterlini, Simple and fast  
542 spectrophotometric determination of H<sub>2</sub>O<sub>2</sub> in photo-Fenton reactions using metavanadate,  
543 Talanta 66 (2005) 86-89.

544 [29] A.D. Eaton, L.S. Clesceri, A.E. Greenberg, M.A.H. Franson, Standard Methodes for  
545 the Examination of Water and Wastewater, twenty-first ed. (2005) APA-AWWA-WEE.

546 [30] N. De la Cruz, R.F. Dantas, J. Giménez, S. Esplugas, Photolysis and TiO<sub>2</sub>  
547 photocatalysis of the pharmaceutical propranolol: solar and artificial light, Applied  
548 Calaysis B: Environmental (2013) 249-256.

549 [31] L.I. Doumic, P.M. Houre, M.C. Cassanello, M.A. Ayude, Mineralization and  
550 efficiency in the homogeneous Fenton Orange G oxidation, Applied Catalysis B:  
551 Environmental 142-143 (2013) 214-221.



552 [32] C. Pulgarin, M. Invernizzi, S. Parra, V. Sarria, R. Polania, P. Péringer, Strategy for  
553 the coupling of photochemical and biological flow reactors useful in mineralization of  
554 biorecalcitrant industrial pollutants, *Catalysis Today* 54 (1999) 341-352.

555 [33] I. Carra, S. Malato, M.201 Jiménez, M.I. Maldonado, J.A. Sánchez Pérez,  
556 Microcontaminant removal by solar photo-Fenton at natural pH run with sequential and  
557 continuous iron additions, *Chemical Engineering Journal* 235 (2014) 132–140.

558 [34] S. Dogruel, T. Olmez-Hanci, Z. Kartal, I. Arslan-Alaton, D. Orhon, Effect of  
559 Fenton's oxidation on the particle size distribution of organic carbon in olive mill  
560 wastewater, *Water Research* 43 (16) (2009) 3974-3983.

561 [35] A. Durán, J.M. Monteagudo, A. Carnicer, Photo-Fenton mineralization of synthetic  
562 apple-juice wastewater, *Chemical Engineering Journal* 168 (1) (2011) 102-107.

563 [36] D. Cassano, A. Zapata, G. Brunetti, G. Del Moro, C. Di Iaconi, I. Oller, S. Malato,  
564 G. Mascolo, Comparison of several combined/integrated biological-AOPs setups for the  
565 treatment of municipal landfill leachate: minimization of operating costs and effluent  
566 toxicity, *Chemical Engineering Journal* 172 (1) (2011) 250-257.

567 [37] J. Rodríguez-Chueca, C. Amor, J.R. Fernandes, P.B. Tavares, M.S. Lucas, J.A.  
568 Peres, Treatment of crystallized-fruit wastewater by UV-A LED photo-Fenton and  
569 coagulation-flocculation, *Chemosphere* 145 (2016) 351-359.

570 [38] J. Bolobajev, E. Kattel, M. Viisimaa, A. Goi, M. Trapido, T. Tenno. N. Dulova,  
571 Reuse of ferric sludge as an iron source for the Fenton-based process in wastewater  
572 treatment 255 (2014) 8-13.

573 [39] A. Brink, C.M. Sheridan, K.G. Harding, The Fenton oxidation of biologically treated  
574 paper and pulp mill effluents: A performance and kinetic study, Process Safety and  
575 Environmental protection 107 (2017) 206-215.

576 [40] G.V.Buxton, C.L. Greenstock, W.P.Helman, A.B.Ross, Critical review of rate  
577 constants for reactions of hydrated electrons, hydrogen atoms and hydroxyl radicals  
578 ( $\cdot\text{OH}/\cdot\text{O}^{\cdot}$ ) in aqueous solution, Journal of Physical and Chemical Reference Data 17  
579 (1988) 513-886.

580

## Supplementary Information for

### Synergies, radiation and kinetics in photo-Fenton process with UVA-LEDs

N. López-Vinent, A. Cruz-Alcalde, L.E. Romero, M.E. Chávez, P. Marco, J. Giménez\*,

S. Esplugas

Department of Chemical Engineering and Analytical Chemistry, Faculty of Chemistry,  
Universitat de Barcelona, C/Martí i Franqués 1, 08028 Barcelona, Spain.

\*Corresponding author:

Jaime Giménez Farreras, phone: +34 934 02 01 54, e-mail: j.gimenez.fa@ub.edu

The SI includes the following 3 figures and 1 table:

#### Table of Contents

<b>Figure S1.</b> The schematic diagram of photoreactor with LEDs on the cover.....	p.2
<b>Figure S2.</b> Fitting of Fig. 2 data to pseudo-first order kinetics for reaction times higher than 30 s and A) wavelength range 380-390 nm, B) wavelength range 380-390 nm and C) wavelength range 380-400 nm .....	p.3
<b>Figure S3.</b> Suggested pathways for DPH degradation in the photo-Fenton experiments.....	p.4
<b>Table S1.</b> Intermediates detected and DPH as an initial compound in photo-Fenton experiments (Rt, retention time).....	p.5

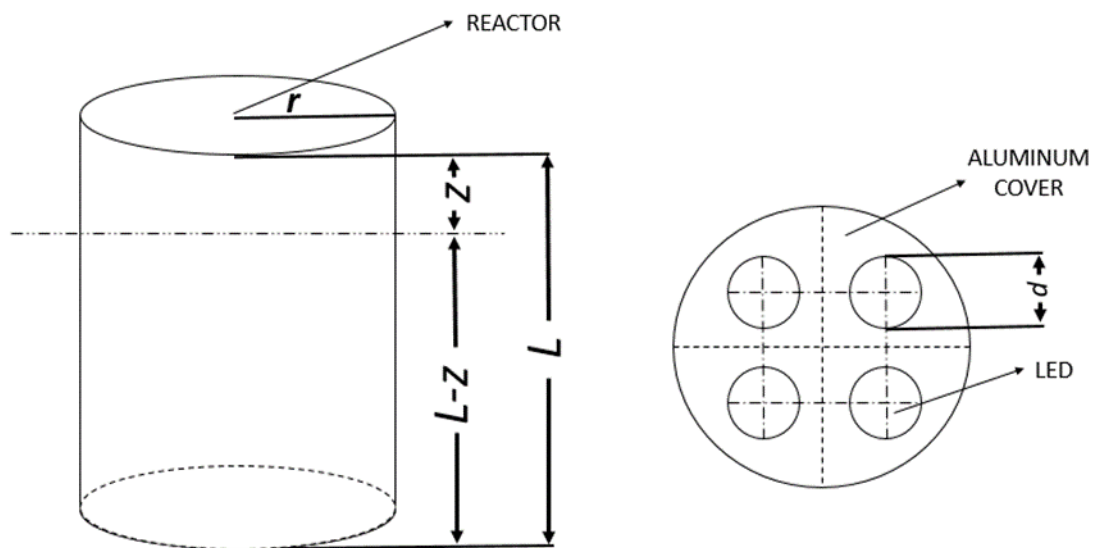


**Figure S1.** The schematic diagram of photoreactor with LEDs on the cover.  $r = 4\text{cm}$ , radius of the photoreactor;  $L = 12\text{cm}$ , photoreactor height;  $z = 3\text{cm}$ , height between aluminum cover and liquid layer;  $d = 3\text{cm}$ , LED diameter. When 380-400 nm were tested LEDs were located crossed.

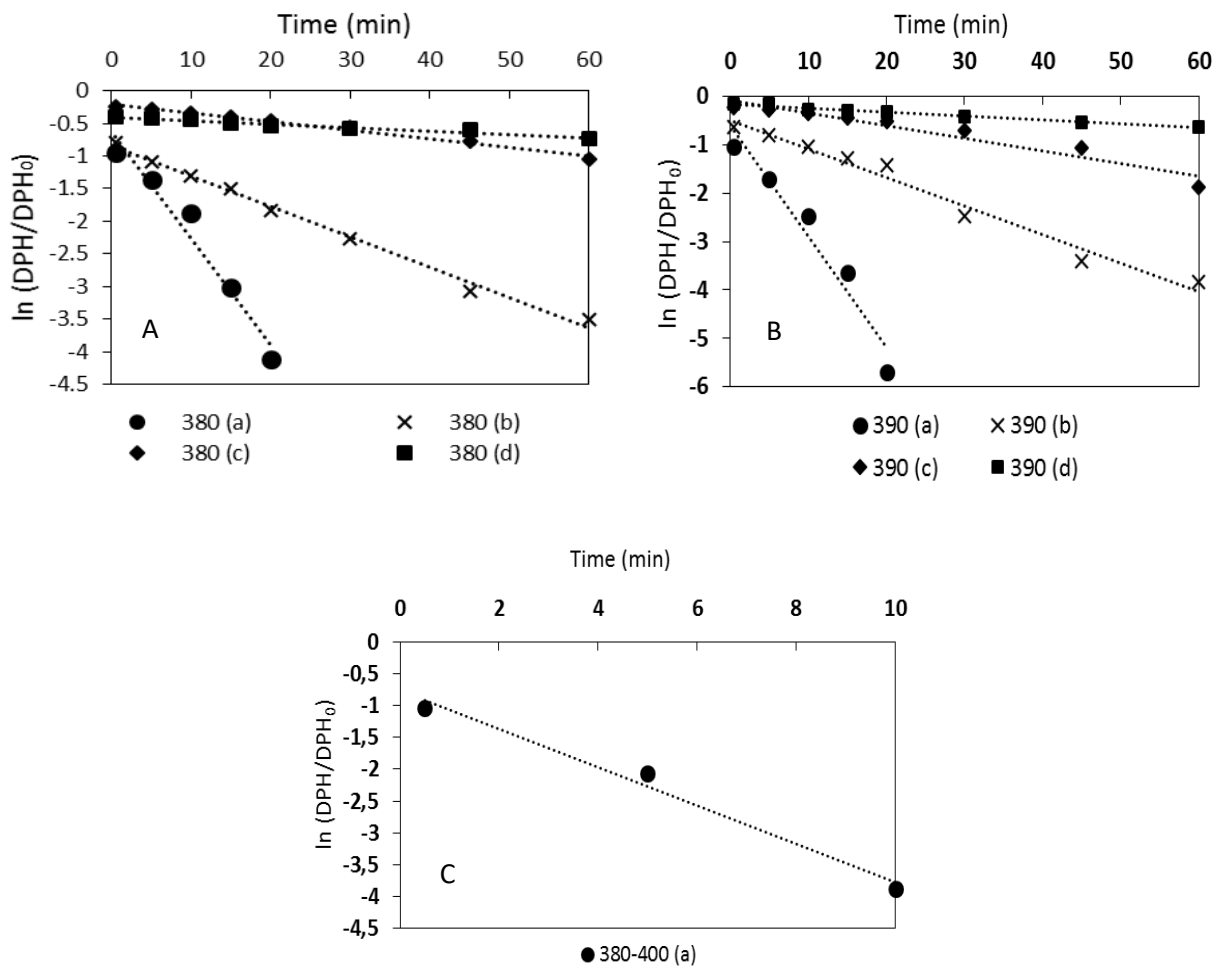


Figure S2. Fitting of Fig. 2 data to pseudo-first order kinetics for reaction times higher than 30 s and A) wavelength range 380-390 nm, B) wavelength range 380-390 nm and C) wavelength range 380-400 nm (a) 10 mg Fe<sup>2+</sup>/L - 150 mg H<sub>2</sub>O<sub>2</sub>/L; (b) 10 mg Fe<sup>2+</sup>/L - 25 mg H<sub>2</sub>O<sub>2</sub>/L; (c) 2.5 mg Fe<sup>2+</sup>/L - 150 mg H<sub>2</sub>O<sub>2</sub>/L; (d) 2.5 mg Fe<sup>2+</sup>/L - 25 mg H<sub>2</sub>O<sub>2</sub>/L.

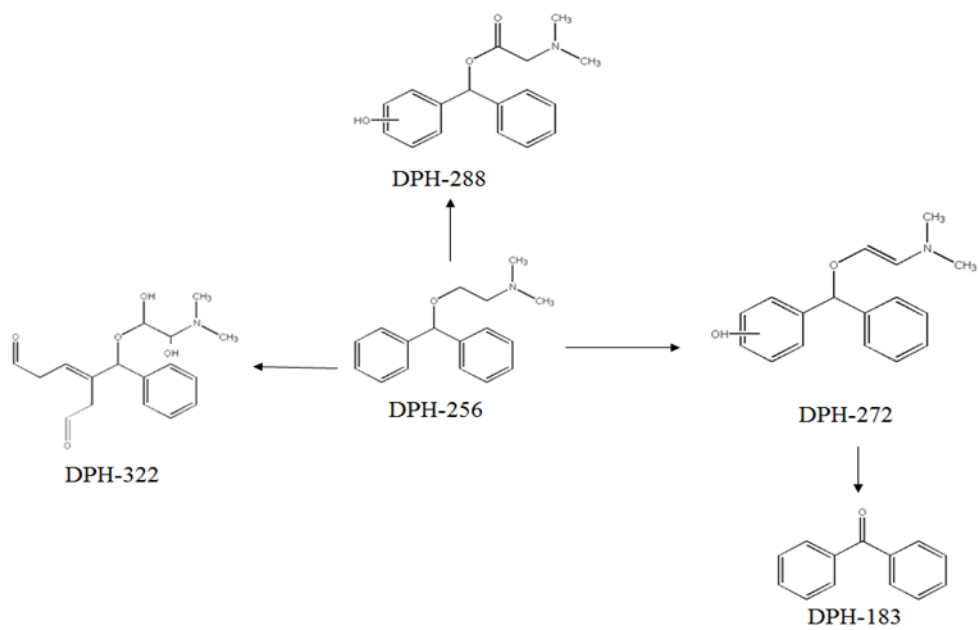
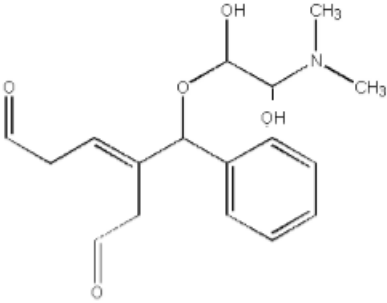
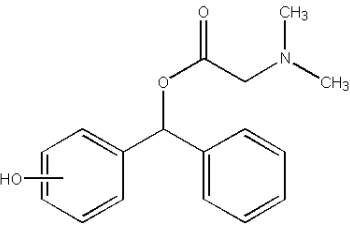
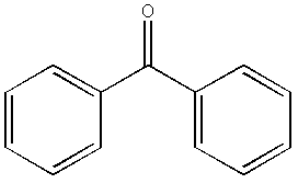
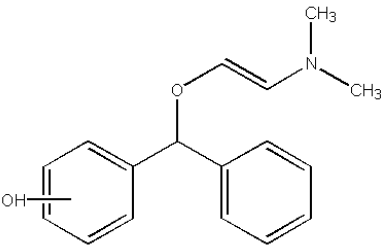
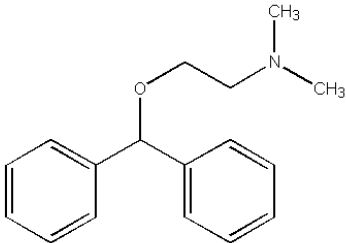


Figure S3. Suggested pathways for DPH degradation in the photo-Fenton experiments.

**Table S1. Intermediates detected and DPH as an initial compound in photo-Fenton experiments (Rt, retention time).**

m/z (Da)	Rt [min]	Elemental composition	Proposed structure
322 (m+1)	1.80	C <sub>17</sub> H <sub>23</sub> NO <sub>5</sub>	 <p style="text-align: center;">DPH-322</p>
288 (m+1)	2.06	C <sub>17</sub> H <sub>21</sub> NO <sub>3</sub>	 <p style="text-align: center;">DPH-288</p>

<b>m/z (Da)</b>	<b>Rt [min]</b>	<b>Elemental composition</b>	<b>Proposed structure</b>
183 (m+1)	2.20	C <sub>13</sub> H <sub>10</sub> O	 <p>DPH-183</p>
272 (m+1)	2.80	C <sub>17</sub> H <sub>21</sub> NO <sub>2</sub>	 <p>DPH-272</p>
256 (m+1)	3.20	C <sub>17</sub> H <sub>21</sub> NO	 <p>DPH (initial compound)</p>